

Local electronic structure of dilute hydrogen in β -Ga₂O₃ probed by muons

M. Hiraishi,^{1,2,*} H. Okabe,^{1,3} A. Koda,^{1,4} R. Kadono,^{1,4,†} T. Ohsawa,⁵ N. Ohashi,⁵ K. Ide,⁶ T. Kamiya,^{6,7} and H. Hosono⁷

¹*Muon Science Laboratory and Condensed Matter Research Center, Institute of Materials Structure Science, High Energy Accelerator Research Organization (KEK-IMSS), Tsukuba, Ibaraki 305-0801, Japan*

²*Graduate School of Science and Engineering, Ibaraki University 2-1-1 Bunkyo, Mito, Ibaraki, 310-8512, Japan.*

³*Institute for Materials Research, Tohoku University (IMR), 2-1-1 Katahira, Aoba-ku, Sendai 980-8577, Japan*

⁴*Department of Materials Structure Science, The Graduate University for Advanced Studies (Sokendai), Tsukuba, Ibaraki 305-0801, Japan*

⁵*National Institute for Materials Science (NIMS), Tsukuba, Ibaraki 305-0044, Japan*

⁶*Materials and Structures Laboratory, Tokyo Institute of Technology, Yokohama, Kanagawa 226-8503, Japan*

⁷*Materials Research Center for Element Strategy, Tokyo Institute of Technology (MCES), Yokohama, Kanagawa 226-8503, Japan*

(Dated: January 6, 2023)

The local electronic structure of muons (Mu) as dilute pseudo-hydrogen in single-crystalline β -Ga₂O₃ has been studied by the muon spin rotation/relaxation (μ SR). High-precision measurements over a long time range of ~ 25 μ s have clearly identified two distinct Mu states: a quasi-static Mu (Mu₁) and fast-moving Mu (Mu₂). By comparing this result with predictions from the recently established ambipolarity model, these two states are respectively attributed to the relaxed-excited states associated with the donor ($E^{+/0}$) and acceptor ($E^{-/0}$) levels predicted by density functional theory (DFT) calculations for the interstitial H. Furthermore, the local electronic structure of Mu₁ is found to be an OMu-bonded state with three-coordinated oxygen. The structure is almost identical with the thermal equilibrium state of H, and it is found to function as an electron donor. The other Mu₂ is considered to be in the hydride state (Mu⁻) from the ambipolarity model, suggesting that it is in fast diffusion motion through the short-lived neutral state due to the charge exchange reaction with conduction electrons (Mu⁰ + e⁻ \rightleftharpoons Mu⁻).

I. INTRODUCTION

Gallium trioxide (β -Ga₂O₃) is attracting attention as a material for high-voltage power devices and other applications because of its large band gap ($E_g \sim 4.9$ eV) and associated high critical electric field [1], where control of electrical activity by p/n -type carrier doping is one of the critical issues. While Sn or Si doping is known to induce n -type conductivity [2, 3], it has been pointed out that impurity hydrogen (H) is the possible cause of unintentional carrier doping in as-grown samples [4].

From infrared spectroscopic studies of β -Ga₂O₃ containing macroscopic amounts of H, a variety of H states including O-H defects have been observed [5, 6]. However, their relationship to carrier doping is not always clear due to the lack of information on their local electronic structures and H valence. Furthermore, since isolated H exists only in trace amounts in solids, experimental means to study its microscopic electronic state are limited. In this regard, theoretical studies based on density functional theory (DFT) calculations have played an important role, and for H in β -Ga₂O₃ DFT calculations have shown that interstitial H may be indeed the origin of n -type doping [7–9]. This prompted us to introduce muons as pseudo-H into β -Ga₂O₃ for investigating the corresponding interstitial H states by analyzing their electronic and dynamical properties in detail by muon spin rotation (μ SR).

The positive muon (μ^+) is an elementary particle with a mass of $0.1126m_p$ (where m_p is the proton mass). The local electronic structure of muon in matter is determined by the muon-electron interaction which is practically equivalent to

H, as can be seen from the fact that the difference in reduced electron mass between a muon-electron bound state (muonium) and a neutral H atom is only 0.43%. Therefore, Mu in matter can be regarded as a light isotope of H ($=^{0.1126}\text{H}$); we introduce the elemental symbol Mu below to denote muon as pseudo-H).

On the other hand, when interpreting the results of the μ SR experiment based on the results of the DFT calculations, there is an important caveat that should be pointed out at this stage. Generally, muons are implanted as an ion beam of relatively high-energy (typically ~ 4 MeV), and the associated electronic excitations in the insulator crystals produce free carriers and excitons ($\sim 10^3$ per muon) [10–12]. These often propagate rapidly in the crystal, and there is experimental evidence that Mu acts as a capture center for them [13]. Consequently, the electronic state of Mu is a relaxed-excited state generated by the interaction with free carriers and excitons, which can be different from the electronic state under thermal equilibrium as expected from the thermodynamic double charge conversion level ($E^{+/-}$) obtained by DFT calculations.

Another well-known evidence that Mu is in a relaxed-excited state is that two or more different electronic states of Mu are often observed simultaneously in the same material [14]. In order to understand the origin of this phenomenon, we have recently conducted an extensive investigation to explore the regularities between the Mu valence states observed in various oxides and the results of previous DFT calculations. As a result, assuming that these relaxed-excited states are associated with acceptor ($E^{0/-}$) and donor ($E^{+/0}$) levels that are predicted by DFT calculations as metastable states, we found that the observed Mu states can be coherently explained by the relationship between acceptor/donor levels and band structure [15]. We call it the “ambipolarity model” since such behavior of Mu is a manifestation of the ambipolarity of

* email: masatoshi.hiraishi.pn93@vc.ibaraki.ac.jp

† email: ryosuke.kadono@kek.jp

H through the relaxed-excited states.

In this study, we show that Mu in single-crystalline β -Ga₂O₃ exhibits two different electronic structures corresponding to the relaxed-excited states respectively associated with the donor and acceptor levels in the ambipolarity model. One is in the OMu-bonded state (Mu₁⁺) corresponding to H serving as a donor, and another is the hydride-like state in rapid motion (Mu₂⁻). In particular, the Mu₂ state is a component overlooked in the previous μ SR experiments [16, 17], and it is speculated to be a transient state diffusing rapidly along the $\langle 010 \rangle$ axis while undergoing the charge exchange reaction, $\text{Mu}_2^- \rightleftharpoons \text{Mu}_2^0 + e^-$. The occurrence of charge exchange is supported by the observation that the temperature dependence of the fractional yield of Mu₂ exhibits a strong correlation with that of the bulk carrier electron mobility and density. This also implies that the interstitial H can take hydride state under electronic excitation and may exhibit fast diffusion motion, depending on the bulk electronic properties of the host.

II. EXPERIMENTAL METHODS AND DFT CALCULATIONS

The sample used in the μ SR experiment was a slab of single crystal (sc-Ga₂O₃, $10 \times 15 \times 0.6 \text{ mm}^3$) with $\langle 001 \rangle$ plane synthesized by the edge-defined film-fed (EFG) method (provided by Novel Crystal Technology, Inc.) [18]. It is reported to have no twin boundary and the lowest carrier density ($N_e \sim 2 \times 10^{17} \text{ cm}^{-3}$) commercially available [18]. The electrical conductivity and Hall effect measurements were performed using the PPMS (Quantum Design Co.). Ohmic contacts were formed from vacuum-deposited Ti at room temperature [19, 20] and gold paste (Seishin Trading Co. LTD., No. 8556). The impurity H content in the sc-Ga₂O₃ sample was estimated to be $3.5 \times 10^{18} \text{ cm}^{-3}$ by thermal desorption spectrometry, which is sufficient to explain the above described N_e . Details are described in Supplemental Material (SM) [21].

In this study, μ SR measurements and data analysis were also performed on a powder sample (99.99%, provided by Rare Metallics Co.) for comparison, and the results were found to be significantly different from those for single crystal. However, these results are excluded from the discussion in this paper, because it is difficult to measure the bulk electronic properties of powder samples which is necessary to consider the cause of the difference. Instead, they are presented with a brief interpretation in SM [21].

Conventional μ SR measurements were performed using the S1 instrument (ARTEMIS) at the Materials and Life-science Experiment Facility, J-PARC [26], where high-precision measurements over a long time range of 20–25 μ s can be routinely performed using a high-flux pulsed muon beam ($\sim 3 \times 10^4 \mu^+/\text{cm}^2/\text{s}$ for the single-pulse mode at a proton beam power of 0.8 MW). The μ SR spectra [the time-dependent decay-positron asymmetry, $A(t)$] which reflects the magnetic field distribution at the Mu site, was measured from room temperature to 4 K under zero field (ZF), weak longitudinal field (LF, parallel to the initial Mu polarization \mathbf{P}_μ), and weak trans-

verse field (TF, perpendicular to \mathbf{P}_μ), and were analyzed by least-squares curve fitting [27]. The background contribution from muons which missed the sample was estimated from μ SR measurements on a holmium plate of the same geometry and subtracted from the asymmetry.

Since the μ SR spectra were found to be dominated by signals from the *diamagnetic* Mu (i.e., Mu⁺ or Mu⁻), the data under ZF/LF conditions were analyzed using the dynamical Kubo-Toyabe (KT) function, $G_z^{\text{KT}}(t; \Delta, \nu, B_{\text{LF}})$, where Δ is the linewidth determined by random local fields from nuclear magnetic moments, B_{LF} is the magnitude of LF, and ν is the fluctuation rate of Δ [28]. The KT function is expressed analytically in the case of static ($\nu = 0$) and ZF ($B_{\text{LF}} = 0$) conditions,

$$G_z^{\text{KT}}(t; \Delta, 0, 0) = \frac{1}{3} + \frac{2}{3} (1 - \Delta^2 t^2) e^{-\frac{1}{2} \Delta^2 t^2}, \quad (1)$$

The magnitude of Δ for a given Mu site is evaluated by calculating the second moments of dipolar fields from nuclear magnetic moments by the following equation,

$$\Delta^2 \simeq \gamma_\mu^2 \sum_m f_m \sum_j \sum_{\alpha=x,y} \sum_{\beta=x,y,z} \gamma_m^2 (\hat{\mathbf{A}}_{mj} \mathbf{I}_m)^2 \sin^2 \Theta_j \quad (2)$$

$$\hat{\mathbf{A}}_{mj} = A_{mj}^{\alpha\beta} = (3r_{mj}^\alpha r_{mj}^\beta - \delta_{\alpha\beta} r_{mj}^2) / r_{mj}^5 \quad (\alpha, \beta = x, y, z)$$

where $\gamma_\mu/2\pi = 135.539 \text{ [MHz/T]}$ is the muon gyromagnetic ratio, $\mathbf{r}_{mj} = (x_{mj}, y_{mj}, z_{mj})$ is the position vector from the muon site to the j -th nucleus, $\boldsymbol{\mu}_m = \gamma_m \mathbf{I}_m$ is the nuclear magnetic moment of the atom with the natural abundance of f_m , Θ_j is the polar angle of \mathbf{r}_{mj} [28]. Since ⁶⁹Ga with $f_1 = 0.604$ and ⁷¹Ga with $f_2 = 0.396$ have nuclear spins of $I_m = 3/2$, respectively, they have electric quadrupole moments. In this case, $\boldsymbol{\mu}_m$ is subject to electric quadrupolar interactions with the electric field gradient generated by the point charge of the diamagnetic Mu, leading to the reduction of the effective $\boldsymbol{\mu}_m$ (by a factor $\sin^2 \Theta_j$) and to the modification of Δ that depends on the initial muon spin direction relative to the crystal axis. (In the powder sample, the spatial averaging leads to $\langle \sin^2 \Theta_j \rangle = 2/3$.) The Δ of the candidate Mu sites inferred from DFT calculations were evaluated using the Dipolec code [29] with Eq. (2) implemented.

DFT calculations were performed to investigate in detail the local structure of H-related defects using OpenMX [25] and VASP codes [23]. Structural relaxation calculations with H (to mimic Mu) using the GGA-PBE exchange correlation function were performed on a $1 \times 3 \times 2$ superlattice with cut-off energies of 200 Ry for OpenMX (520 eV for VASP), and K points were set to $3 \times 4 \times 3$. Structures were relaxed until the the maximum force on each atom was less than 3×10^{-4} (Hartree/Bohr) for OpenMX (0.01 eV/Å for VASP). Additional structural relaxation calculations using the Heyd-Scuseria-Ernzerhof (HSE06) hybrid functional implemented in VASP were performed with K points of $2 \times 3 \times 2$ to confirm the structure of the minimum formation energy [24]. The Hartree-Fock mixing parameter was set to 0.35, which reproduces the experimental value of the band gap [7, 8].

III. RESULTS

First, we investigated the initial asymmetry [$A(0)$] of the μ SR spectrum under $TF = 2$ mT and found that it is independent of temperature (T) and nearly constant within experimental error over the entire measured temperature range $4 \leq T \leq 300$ K [see Fig. S5(a) in SM [21]]. Since the absence of a paramagnetic Mu at 300 K is confirmed from the TF data, the T -independent $A(0)$ values indicates that the muon is mostly in diamagnetic state(s) at all temperatures. (For the possibility of Mu^0 with extremely small hyperfine parameters to exist, see Section IV.)

The normalized μ SR time spectra [$G_z(t) \equiv A(t)/A(0)$] at 300 K under ZF and LF ($\parallel \langle 001 \rangle$) are shown in Fig. 1(a). The ZF- μ SR spectrum shows that it consists of two components, one we call Mu_1 , which partially recovers at $t \geq 12$ μ s following slow Gaussian relaxation, and Mu_2 , which exhibits almost no relaxation. Note that the recovery of $G_z(t)$ characteristic to the 1/3-tail of the Kubo-Toyabe function in Eq. (1) is clearly visible only for $t \geq 15$ μ s. This could not have been detectable by previous μ SR measurements under TF alone [16] or those using a continuous muon beam [17], and has been first revealed by precise ZF- μ SR measurements using the high-flux pulsed muon beam at J-PARC. The suppression of the Gaussian relaxation by the weak LF indicates that the relaxation for the Mu_1 component is induced by the quasi-static random local fields from Ga nuclear magnetic moments.

It is clear from Fig. 1(b) that the relative yield of Mu_1 vs

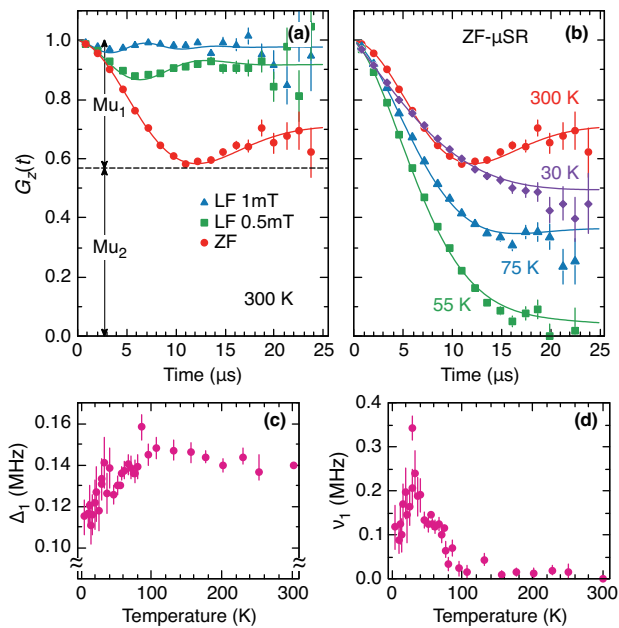


FIG. 1. (a) ZF and LF μ SR time spectra observed at 300 K (4.0×10^8 positron events collected for ZF and 2.0×10^8 for LF), which consists of two components (Mu_1 and Mu_2). (b) ZF spectra at typical temperatures (3.0×10^8 positron events collected). The solid curves represent the least-square fit by Eq. (3). The horizontal dashed line shows f_2 . (c), (d) Temperature dependence of the linewidth Δ_1 and fluctuation rate ν_1 for the Mu_1 component.

Mu_2 apparently depends on T at lower temperatures. Furthermore, the lineshape exhibits change from a Gaussian to exponential-like behavior at low temperatures [see $G_z(t)$ for $t \lesssim 6$ μ s at 30 K]. Considering these features, we analyzed the ZF and LF spectra by global curve-fits using the following function,

$$G_z(t) = f_1 G_z^{\text{KT}}(t; \Delta_1, \nu_1, B_{\text{LF}}) e^{-\lambda t} + f_2, \quad (3)$$

where f_i ($i = 1, 2$) are the relative yields of the Mu_i components. The exponential damping with the relaxation rate λ is introduced to describe the possible influence of the fluctuating magnetic fields from unpaired electrons (including excited carriers and excitons localized nearby Mu). As shown by the solid lines in Figs. 1(a) (b), curve fit using Eq. (3) provides reasonable agreement with the data, and $\Delta_1 = 0.140(1)$ MHz is obtained from the fit at 300 K. The T dependencies of Δ_1 and ν_1 obtained from the fit are shown in Figs. 1(c) and (d), and those of f_2 and λ in Figs. 2(a) and (c), respectively.

Above $T_\gamma \simeq 80$ K where the $f_1 (= 1 - f_2)$ is nearly independent of T , Δ_1 , ν_1 and λ also show similar trends; Δ_1 increases slightly to ~ 0.15 MHz as T decreases, while ν_1 and λ shows a constant value close to zero ($\ll \Delta_1$). This indicates that the Mu_1 component is quasistatic for $T \geq T_\gamma$. Meanwhile, the rapid motion of Mu_2 is inferred from the fact that there is no interstitial sites free of local magnetic fields from Ga nuclear magnetic moments (with 100% natural abundance); Δ calculated at any site is always larger than ~ 0.15 MHz for the unrelaxed lattice, which is only compatible with the situation where the relaxation due to the local field (with a linewidth $\Delta_2 \geq 0.15$ MHz) is suppressed by the motional averaging, namely,

$$G_z(t) = f_1 G_z^{\text{KT}}(t; \Delta_1, \nu_1, B_{\text{LF}}) e^{-\lambda t} + f_2 G_z^{\text{KT}}(t; \Delta_2, \nu_2), \quad (4)$$

with $G_z^{\text{KT}}(t; \Delta_2, \nu_2) \simeq 1$ for $\nu_2 \gg \Delta_2$.

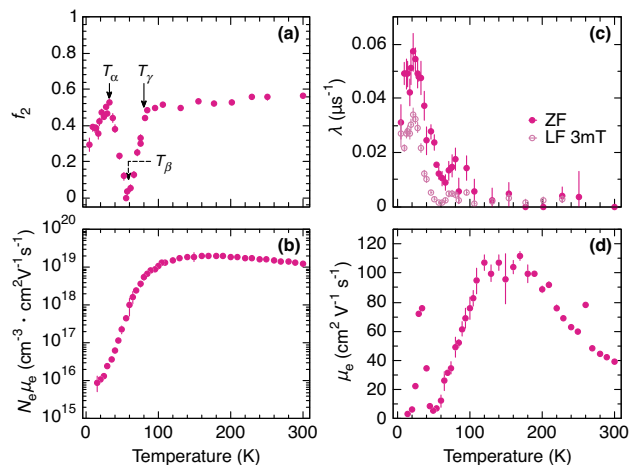


FIG. 2. Temperature dependence of (a) fractional yield for the Mu_2 component [$f_2 \equiv A_2/A(0)$] which is characterized by the changes at $T_\alpha \simeq 30$ K, $T_\beta \simeq 55$ K and $T_\gamma \simeq 80$ K, (b) bulk carrier density (N_e) multiplied by mobility [μ_e , shown in (d)], (c) exponential relaxation rate (λ) at ZF and LF = 3 mT. Note that the vertical axis of (b) is on a logarithmic scale.

Below T_γ , v_1 increases with decreasing T in correlation with f_2 , and tends to approach a constant value or decrease for $T \lesssim T_\alpha \simeq 30$ K. A similar correlation is observed between f_2 and λ ; λ gradually increases with decreasing T to exhibit a small peak around T_γ , then decreases towards T_β , followed by an increase to reach another maximum near T_α . Here, we point out that, as shown in Fig. 2(b), the complicated T dependence of f_2 and the increase of λ occur in correlation with the decrease of $N_e \mu_e$ (with μ_e being the mobility) of the sample used for μ SR measurements. More specifically, N_e exhibits gradual decrease around T_γ with decreasing T , followed by a sharp decrease below T_β and an increase below T_α (see Fig. S2 in SM [21]). As shown in Fig. 2(d), μ_e decreases with decreasing T below ~ 120 K, reaching a minimum around T_β , and then increases to a maximum at T_α . The behavior of μ_e for $T > T_\gamma$ is qualitatively in line with previous reports [30, 31]. This implies that the electronic state of Mu is highly sensitive to the quality of samples, which is also supported by the fact that the T dependence of f_2 (and f_1) in powder sample differs significantly from that in single crystal (see Fig. S5(b) in SM [21]).

IV. DISCUSSION

In the ambipolarity model, the electronic state of the interstitial Mu is determined by where the donor and acceptor levels associated with H, predicted from the Fermi energy (E_F) dependence of defect formation energy (Ξ^q) for H^q ($q = \pm, 0$), is located in the energy band structure of the host material. Figure 3(a) shows $\Xi^q(E_F)$ for each valence state of H obtained by previous DFT calculations [9], where H is substituted with Mu. The relationship between the donor/acceptor levels and band structure predicts that Mu can take two different diamagnetic states: a donor-like state in which it releases an electron into the conduction band to become Mu^+ , and a hydride (Mu^-) state, which is qualitatively consistent with the present observations. Interestingly, the $E^{+/-}$ level, which determines the charge state of H at thermal equilibrium, is in the conduction band as is the donor level, so the behavior of H is expected to be the same as that of the donor-like Mu.

To determine the local defect structure of the Mu_1 state, Δ_1 was compared with those calculated for the candidate sites, and the results are summarized in Table I. The value for the

TABLE I. Comparison of the linewidth (Δ) between those at the H sites obtained from structural relaxation calculations and the experimental value. Δ_{sc} , and Δ_{pwr} for single crystalline (sc) and powder (pwr) samples, respectively. d_{OH} is the distance from H to the nearest oxygen (see also Fig. 4).

Site	d_{OH} [nm]	Δ_{sc} (MHz)	Δ_{pwr} (MHz)
H _I	0.0966	0.136	0.137
H _{II}	0.1036	0.150	0.153
H _{III}	0.1003	0.161	0.156
H ⁻	-	0.345	0.299
Δ_1 (300 K)		0.140(1)	0.136(1)

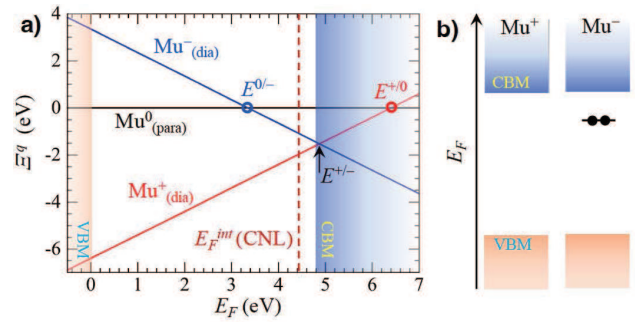


FIG. 3. a) The formation energy (Ξ^q) of interstitial Mu (Mu_1^q , $q = 0, \pm$) vs the Fermi level (E_F) in β -Ga₂O₃ inferred from DFT calculations for H^q [9]. The donor/acceptor levels are determined as cross points between $\Xi^\pm(E_F)$ and $\Xi^0(E_F)$. The dashed line shows the intrinsic charge neutral level (E_F^{int}) obtained from the DFT calculation. b) Schematic band diagrams for the electron energy associated with the donor/acceptor levels in a).

H_I site bonded to the three-coordinated O_I [see Fig. 4(a)] is in good agreement with Δ_1 at 300 K, indicating that $H_1^+ \approx Mu_1^+$ in the dilute limit ($\sim 10^5$ cm⁻³). This confirms the earlier point that, aside from not knowing the exact location of $E^{+/-}$, H_I can serve as donor [8]. The existence of H in the H_I structure has been also inferred from the infrared spectroscopy of hydrogenated β -Ga₂O₃ [6]. The possibility that Mu_1 corresponds to H trapped in Ga and O vacancies is excluded by the comparison of Δ_1 with those for Mu in these vacancies (shown in Table S1 in SM [21]).

As seen in Fig. 1(c), Δ_1 exhibits a slight increase with decreasing T , approaching the value at the H_{II}/H_{III} sites [see Fig. 4(b), (c)]. This can be interpreted as reflecting the fact that the initial population of relaxed-excited states immediately after muon implantation is a random sampling of available metastable sites. Considering that the difference in the formation energy estimated by DFT calculations is small among these sites (e.g., ~ 30 meV between H_I and H_{II}), the decrease in Δ_1 with increasing T above T_γ suggests that the Mu site distribution approaches the lowest energy state by the annealing process. A similar T dependence of Δ exhibited by donor-like Mu has been reported for InGaZnO₄ in which multiple H sites are available [32].

With Mu_1 identified as being in the donor-like state, the paired Mu_2 component is presumed to be in the acceptor-like diamagnetic state (Mu_2^-) from the ambipolarity model. According to DFT calculations, the corresponding H⁻ state is bonded to the two nn Ga ions, as shown in Fig. 4(d) [9]. The $E^{0/-}$ level is near the conduction band, and it can still accommodate two electrons as it is located below the charge neutral level (E_F^{int} , see Fig. 3). This means that it is possible for Mu_2 to exchange electrons with the conduction band. Moreover, the conduction band has a relatively large dispersion (effective mass $\sim 0.28m_e$) around the Γ point [33], allowing fast migration of electrons.

While Mu_2^- is unlikely to exhibit fast diffusion by itself due to the bonding to cations, there are many reported examples of fast diffusive motion of acceptor-like Mu^0 in semiconduc-

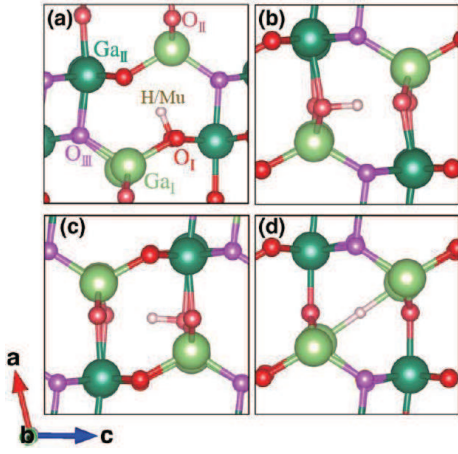


FIG. 4. Local structures H-related defects corresponding to (a) H_I , (b) H_{II} , (c) H_{III} and (d) H^- state. H_{I-III} are bonded to O, while H^- forms bonding with two Ga^{3+} ions [9]. The crystal structures were displayed using VESTA [22].

tors and alkali halides [34–37]. Since $N_e\mu_e$ and f_2 show almost the same T dependence for $T > T_\beta$, it is inferred that the Mu_2 state diffuses rapidly for $T > T_\gamma$ through the neutral state temporarily attained by the charge exchange reaction $Mu_2^- \rightleftharpoons Mu_2^0 + e^-$. The reaction rate is given by

$$r_{ex} = \frac{1}{\tau_{-0} + \tau_{0-}} = \frac{r_{-0}r_{0-}}{r_{-0} + r_{0-}}, \quad (5)$$

where r_{-0} ($= 1/\tau_{-0}$) is the ionization probability ($\propto e^{-\Delta E/k_B T}$, with $\Delta E \sim E_c - E^{0/-}$ and E_c the CBM energy) and r_{0-} ($= 1/\tau_{0-}$) is the capture rate of the free carriers ($\propto \sigma_c N_e \mu_e V_r$, with σ_c , μ_e , and V_r being the cross section, carrier mobility, and electric field exerted from the Mu-Ga complex state, respectively). Note that λ due to the charge exchange is also quenched by the motional averaging when r_{ex} is much greater than the hyperfine parameter. Such motional effects have also been observed in SiO_2 and are thought to be responsible for the disappearance of anisotropy in the hyperfine interaction of Mu^0 with increasing T [37]. The existence of the non-relaxing Mu component has also been reported for variety of materials including $NaAlH_4$, $LaScSiH_x$, and FeS_2 [38–40], implying the ubiquitous nature of acceptor-like Mu states.

It is natural to assume that Mu_2 diffuses along the $\langle 010 \rangle$ direction because β - Ga_2O_3 has an open channel structure along the $\langle 010 \rangle$ direction. In fact, secondary ion mass spectrometry analysis of 2H implanted β - Ga_2O_3 [41] revealed that 2H diffuses more easily in the $\langle 010 \rangle$ direction than perpendicular to the $\langle -201 \rangle$ surface. It has also been reported for rutile TiO_2 that hydrogen diffusion is more likely to occur in open channels along the c -axis than in the a - b plane [42].

There are three different open channels in the $\langle 010 \rangle$ direction in β - Ga_2O_3 . The potentials associated with diffusion in each channel were investigated by total energy calculations (see Sect. III in SM [21] for details), and it was found that hydrogen tends to diffuse in the same channel as the Mu_1 site.

Since the two charged states Mu_1^+ and Mu_2^- accompany mutually different lattice distortions, it is assumed that the potential barriers caused by these distortions allow Mu_2 to diffuse while maintaining its state. However, because the adopted calculations do not take structural relaxation into account, it is a future task to evaluate using the nudged-elastic band (NEB) method.

The details of what causes the decrease in f_2 (increase in f_1) and recovery below T_γ , which is apparently correlated with the onset of slow dynamics for Mu_1 (as inferred from the T dependence of Δ_1 , v_1 , and λ), are currently unknown. Nevertheless, when analyzing the time spectra in this T range using Eq. (4) with Δ_1 and Δ_2 as free parameters, Δ_i converge to mutually close values (~ 0.13 – 0.14 MHz). A curve fit performed with Δ_1 fixed at 0.136 MHz and Δ_2 at 0.345 MHz (corresponding to the stationary hydride state) and the other parameters free fails to reproduce the data, as indicated by a large reduced chi-square (see Fig. S6 in SM). Thus, the decrease in f_2 suggests that a transition from Mu_2 to Mu_1 occurs in the relevant T range. One possible scenario is that Mu_2^- can be ionized by thermal excitation and transitions to Mu_1^+ for $T < T_\beta$, but the ionization is prevented by increasing $N_e\mu_e$ for $T > T_\beta$ [i.e., $r_{0-} \gg r_{-0}$ in Eq. (5)], allowing it to continue to exist as a metastable state again above T_γ .

Finally, we comment on the relationship between our experimental results and the prior μ SR studies on β - Ga_2O_3 . In Ref. [16], TF- μ SR measurements are reported for a powder sample from a commercial vendor, and it is observed that about 10% of the signal exhibits slight increase of relaxation rate from 0.08 MHz to 0.12 MHz below 50–100 K. Ref. [17] reports results for a single-crystal sample (orientation unknown) and observes a 4–6% decrease in the initial asymmetry below 50–100 K in both ZF and TF- μ SR measurements and an increase in Δ of the component described by $G_z^{KT}(t)$ from 0.10–0.11 MHz to 0.15 MHz in the ZF- μ SR spectra. Although detailed comparisons with our results are not possible because no time spectra are available for either case, these changes appear to correspond to the increase in f_1 at $T < T_\gamma$ that we observed in both the powder and single-crystalline samples [see Fig. S5(b) in SM [21]]. Meanwhile, these reports are silent about the component corresponding to Mu_2 . We stress that the existence and origin of Mu_2 are clearly identified for the first time in this study with the help of the ambipolarity model.

ACKNOWLEDGMENTS

This work was supported by the MEXT Elements Strategy Initiative to Form Core Research Center for Electron Materials (Grant No. JPMXP0112101001) and JSPS KAKENHI (Grant No. 19K15033). The μ SR experiments were conducted under user programs (Proposal No. 2019MS02) at the Materials and Life Science Experimental Facility of the J-PARC. We also acknowledge the Neutron Science and Technology Center, CROSS for the use of PPMS in their user laboratories.

- [1] Z. Galazka, “ β -Ga₂O₃ for wide-bandgap electronics and optoelectronics,” *Semicond. Sci. Technol.* **33**, 113001 (2018).
- [2] N. Ueda, H. Hosono, R. Waseda, and H. Kawazoe, “Synthesis and control of conductivity of ultraviolet transmitting β -Ga₂O₃ single crystals,” *Appl. Phys. Lett.* **70**, 3561–3563 (1997).
- [3] M. Orita, H. Ohta, M. Hirano, and H. Hosono, “Deep-ultraviolet transparent conductive β -Ga₂O₃ thin films,” *Appl. Phys. Lett.* **77**, 4166–4168 (2000).
- [4] Z. Galazka, K. Irmscher, R. Schewski, I. M. Hanke, M. Pietsch, S. Ganschow, D. Klimm, A. Dittmar, A. Fiedler, T. Schroeder, and M. Bickermann, “Czochralski-grown bulk β -Ga₂O₃ single crystals doped with mono-, di-, tri-, and tetravalent ions,” *J. Cryst. Growth* **529**, 125297 (2020).
- [5] P. Weiser, M. Stavola, W. B. Fowler, Y. Qin, and S. Pearton, “Structure and vibrational properties of the dominant O-H center in β -Ga₂O₃,” *Appl. Phys. Lett.* **112**, 232104 (2018).
- [6] Y. Qin, M. Stavola, W. B. Fowler, P. Weiser, and S. J. Pearton, “Hydrogen centers in β -Ga₂O₃: Infrared spectroscopy and density functional theory,” *ECS J. Solid State Sci. Technol.* **8**, Q3103–Q3110 (2019).
- [7] J. B. Varley, J. R. Weber, A. Janotti, and C. G. Van de Walle, “Oxygen vacancies and donor impurities in β -Ga₂O₃,” *Appl. Phys. Lett.* **97**, 142106 (2010).
- [8] J. B. Varley, H. Peelaers, A. Janotti, and C. G. Van de Walle, “Hydrogenated cation vacancies in semiconducting oxides,” *J. Phys. Condens.: Matter* **23**, 334212 (2011).
- [9] H. Li and J. Robertson, “Behaviour of hydrogen in wide band gap oxides,” *J. Appl. Phys.* **115**, 203708 (2014).
- [10] M. W. Thompson, *Defects and Radiation Damage in Metals*, Cambridge Monographs on Physics (Cambridge University Press, Cambridge, 1974).
- [11] R. C. Alig and S. Bloom, “Electron-hole-pair creation energies in semiconductors,” *Phys. Rev. Lett.* **35**, 1522–1525 (1975).
- [12] N. Itoh, “Bond scission induced by electronic excitation in solids: A tool for nanomanipulation,” *Nucl. Instr. Meth. Phys. Res. B* **122**, 405–409 (1997).
- [13] T. Prokscha, E. Morenzoni, D. G. Eshchenko, N. Garifianov, H. Glückler, R. Khasanov, H. Luetkens, and A. Suter, “Formation of hydrogen impurity states in silicon and insulators at low implantation energies,” *Phys. Rev. Lett.* **98**, 227401 (2007).
- [14] R. L. Lichti, K. H. Chow, and S. F. J. Cox, “Hydrogen defect-level pinning in semiconductors: The muonium equivalent,” *Phys. Rev. Lett.* **101**, 136403 (2008).
- [15] M. Hiraishi, H. Okabe, A. Koda, R. Kadono, and H. Hosono, “Ambipolarity of diluted hydrogen in wide-gap oxides revealed by muon study,” *J. Appl. Phys.* **132**, 105701 (2022).
- [16] P. D. C. King, I. McKenzie, and T. D. Veal, “Observation of shallow-donor muonium in Ga₂O₃: Evidence for hydrogen-induced conductivity,” *Appl. Phys. Lett.* **96**, 062110 (2010).
- [17] Y. G. Celebi, R. L. Lichti, B. B. Baker, P. W. Mengyan, and H. N. Bani-Salameh, “Motion of Mu⁺ in transparent conducting oxides,” *Phys. Proc.* **30**, 206–209 (2012).
- [18] A. Kuramata, K. Koshi, S. Watanabe, Y. Yamaoka, T. Masui, and S. Yamakoshi, “High-quality β -Ga₂O₃ single crystals grown by edge-defined film-fed growth,” *Jpn. J. Appl. Phys.* **55**, 1202A2 (2016).
- [19] E. G. Villora, K. Shimamura, T. Ujiie, and K. Aoki, “Electrical conductivity and lattice expansion of β -Ga₂O₃ below room temperature,” *Appl. Phys. Lett.* **92**, 202118 (2008).
- [20] K. Irmscher, Z. Galazka, M. Pietsch, R. Uecker, and R. Fornari, “Electrical properties of β -Ga₂O₃ single crystals grown by the Czochralski method,” *J. Appl. Phys.* **110**, 063720 (2011).
- [21] See Supplemental Material at [URL will be inserted by publisher] for details on sample characterization by TDS and Hall coefficient measurements, DFT calculations for muon sites, μ SR results for a powder sample, and on the comparison of curve fits for the μ SR spectra around T_{β} .
- [22] K. Momma and F. Izumi, “VESTA3 for three-dimensional visualization of crystal, volumetric and morphology data,” *J. Appl. Crystallogr.* **44**, 1272–1276 (2011).
- [23] G. Kresse and J. Hafner, “Ab initio molecular dynamics for liquid metals,” *Phys. Rev. B* **47**, 558–561 (1993).
- [24] A. V. Krukau, O. A. Vydrov, A. F. Izmaylov, and G. E. Scuseria, “Influence of the exchange screening parameter on the performance of screened hybrid functionals,” *J. Chem. Phys.* **125**, 224106 (2006).
- [25] T. Ozaki, “Variationally optimized atomic orbitals for large-scale electronic structures,” *Phys. Rev. B* **67**, 155108 (2003).
- [26] K. M. Kojima, T. Murakami, Y. Takahashi, H. Lee, S. Y. Suzuki, A. Koda, I. Yamauchi, M. Miyazaki, M. Hiraishi, H. Okabe, S. Takeshita, R. Kadono, T. Ito, W. Higemoto, S. Kanda, Y. Fukao, N. Saito, M. Saito, M. Ikeno, T. Uchida, and M. M. Tanaka, “New μ SR spectrometer at J-PARC MUSE based on Kalliope detectors,” *J. Phys.: Conf. Ser.* **551**, 012063 (2014).
- [27] A. Suter and B.M. Wojek, “Musrfit: A free platform-independent framework for μ sr data analysis,” *Phys. Proc.* **30**, 69–73 (2012).
- [28] R. S. Hayano, Y. J. Uemura, J. Imazato, N. Nishida, T. Yamazaki, and R. Kubo, “Zero- and low-field spin relaxation studied by positive muons,” *Phys. Rev. B* **20**, 850–859 (1979).
- [29] K. M. Kojima, private communication.
- [30] A. Parisini and R. Fornari, “Analysis of the scattering mechanisms controlling electron mobility in β -Ga₂O₃ crystals,” *Semicond. Sci. Technol.* **31**, 035023 (2016).
- [31] Z. Kabilova, C. Kurdak, and R. L. Peterson, “Observation of impurity band conduction and variable range hopping in heavily doped (010) β -Ga₂O₃,” *Semicond. Sci. Technol.* **34**, 03LT02 (2019).
- [32] K. M. Kojima, M. Hiraishi, H. Okabe, A. Koda, R. Kadono, K. Ide, S. Matsuishi, H. Kumomi, T. Kamiya, and H. Hosono, “Electronic structure of interstitial hydrogen in In-Ga-Zn-O semiconductor simulated by muon,” *Appl. Phys. Lett.* **115**, 122104 (2019).
- [33] H. Peelaers and C. G. Van de Walle, “Brillouin zone and band structure of β -Ga₂O₃,” *Phys. Status Solidi (b)* **252**, 828–832 (2015).
- [34] B. D. Patterson, “Muonium states in semiconductors,” *Rev. Mod. Phys.* **60**, 69–159 (1988).
- [35] R. Kadono, A. Matsushita, K. Nagamine, K. Nishiyama, K. H. Chow, R. F. Kiefl, A. MacFarlane, D. Schumann, S. Fujii, and S. Tanigawa, “Charge state and diffusivity of muonium in n-type GaAs,” *Phys. Rev. B* **50**, 1999–2002 (1994).
- [36] D. Gxawu, I. Z. Machi, S. H. Connell, K. Bharuth-Ram, M. J. Sithole, and S. F. J. Cox, “Diffusion of interstitial muonium, Mu_i, in a ¹³C diamond,” *Diamond Relat. Mater.* **14**, 375–379 (2005).
- [37] K. H. Chow, R. F. Kiefl, B. Hitti, T. L. Estle, and R. L. Lichti, “Novel behavior of bond-centered muonium in heavily doped n-type silicon: Curie-like spin susceptibility and charge screening,” *Phys. Rev. Lett.* **84**, 2251–2254 (2000).
- [38] R. Kadono, K. Shimomura, K. H. Satoh, S. Takeshita, A. Koda, K. Nishiyama, E. Akiba, R. M. Ayabe, M. Kuba, and C. M.

- Jensen, “Hydrogen bonding in sodium alanate: A muon spin rotation study,” *Phys. Rev. Lett.* **100**, 026401 (2008).
- [39] H. Okabe, M. Hiraishi, S. Takeshita, A. Koda, K. M. Kojima, and R. Kadono, “Local electronic structure of interstitial hydrogen in iron disulfide,” *Phys. Rev. B* **98**, 075210 (2018).
- [40] M. Hiraishi, K. M. Kojima, H. Okabe, A. Koda, R. Kadono, J. Wu, Y. Lu, and H. Hosono, “Anomalous diamagnetism of electride electrons in transition metal silicides,” *Phys. Rev. B* **103**, L241101 (2021).
- [41] V. M. Reinertsen, P. M. Weiser, Y. K. Frodason, M. E. Bathen, L. Vines, and K. M. Johansen, “Anisotropic and trap-limited diffusion of hydrogen/deuterium in monoclinic gallium oxide single crystals,” *Appl. Phys. Lett.* **117**, 232106 (2020).
- [42] J. B. Bates, J. C. Wang, and R. A. Perkins, “Mechanisms for hydrogen diffusion in TiO_2 ,” *Phys. Rev. B* **19**, 4130–4139 (1979).

Supplemental Material: Local electronic structure of dilute hydrogen in β -Ga₂O₃ probed by muons

M. Hiraishi *et al.*

I. PROPERTIES OF SINGLE CRYSTALLINE β -Ga₂O₃

A. Thermal Desorption Spectrometry (TDS)

Figure S1 shows the TDS results for the $\langle 001 \rangle$ sample, which was linearly heated from room temperature to 800°C and held at 800°C for 1 hour. Temperature is shown on the right axis and the signal intensities obtained by the quadrupole mass spectrometer (QMS) are shown on the left vertical axis. The analysis revealed that the $\langle 001 \rangle$ sample contains $3.5 \times 10^{18} \text{cm}^{-3}$ of hydrogen ($m/z = 2$, with m being the mass number, z the ion valence). Considering that the desorption process is diffusion-limited for crystalline specimens, this value may correspond to the lower limit. The signal intensity for $m/z = 18$ ($^1\text{H}_2^{16}\text{O}$, ^{18}O) is greater than that for $m/z = 16$ (^{16}O) multiplied by 0.002 (natural abundance of ^{18}O), indicating that $m/z = 18$ is derived from water (H_2O). The similar temperature dependence of $m/z = 1$ and 17 to that of 18 strongly suggests that $m/z = 1, 17$ are also water-related signals. The steep increase below 100°C (~ 20 min.) is probably due to residual moisture on the sample surface, chamber, and so on.

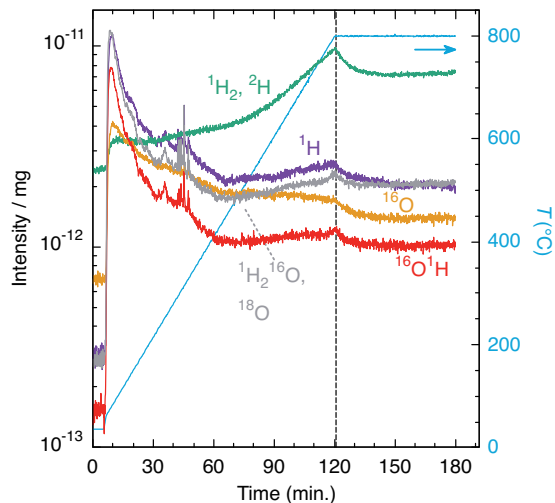


FIG. S1. TDS spectra of the β -Ga₂O₃ sample used for μ SR measurements. Purple, green, yellow, red, and gray are signals for $m/z = 1, 2, 16, 17$, and 18, respectively (m : mass number, z : ion valence). Temperature history is shown on the right vertical axis.

B. Carrier concentration

The temperature dependence of carrier concentration obtained from Hall coefficient measurements for the β -Ga₂O₃

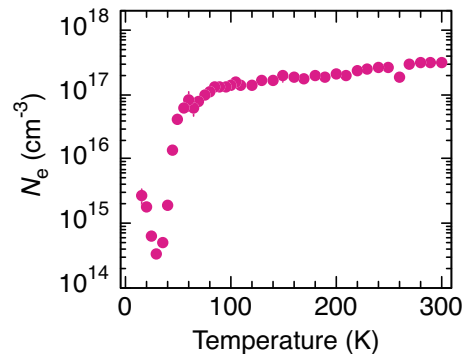


FIG. S2. Temperature dependence of the electron carrier concentration in the single crystalline sample of β -Ga₂O₃.

sample (with $\langle 001 \rangle$ orientation) used for μ SR measurements is shown in Fig. S2. The sign of the Hall coefficient indicates that majority carriers are electrons.

II. RESULT OF DFT CALCULATIONS

The relaxed structures obtained by DFT calculations are shown in Fig. S3, and the simulated muon spin relaxation rates Δ in the Kubo-Toyabe function for each structure are shown in Table S1.

TABLE S1. The nuclear dipolar linewidth Δ for the various local structures involving interstitial H obtained from structural relaxation calculations. \star indicate the results of VASP:HSE06 calculations [23, 24], while others were those by OpenMX:GGA-PBE [25]. d_{OH} denotes the distance between H and the nearest O. $\Delta_{(001)}$ and Δ_{pwr} are the linewidths for single crystalline and powder samples, respectively.

Type	Config.	nn oxygen	d_{OH} (nm)	$\Delta_{(001)}$ (MHz)	Δ_{pwr} (MHz)
Interstitial \star	H _I	O _I	0.0966	0.136	0.137
Interstitial \star	H _{II}	O _{II}	0.1036	0.150	0.153
Interstitial \star	H _{III}	O _{II}	0.1003	0.161	0.158
Interstitial	H _{IV}	O _{III}	0.1024	0.157	0.165
Interstitial	H _V	O _{III}	0.0996	0.158	0.170
Interstitial	H _{VI}	O _I	0.0989	0.175	0.162
Vacancy	V _{Ga_I} -H	O _I	0.0983	0.106	0.117
Vacancy	V _{Ga_{II}} -H	O _I	0.0988	0.108	0.115
Vacancy	V _{O_I} -H	—	—	0.286	0.250
Vacancy	V _{O_{II}} -H	—	—	0.168	0.235
Vacancy	V _{O_{III}} -H	—	—	0.229	0.238

III. $\langle 010 \rangle$ AXIAL DIFFUSION: EVALUATION BASED ON TOTAL ENERGY.

To investigate the Mu₂ diffusion path, $\langle 010 \rangle$ axis position y dependence of the total energy E_{tot} was calculated in a $1 \times$

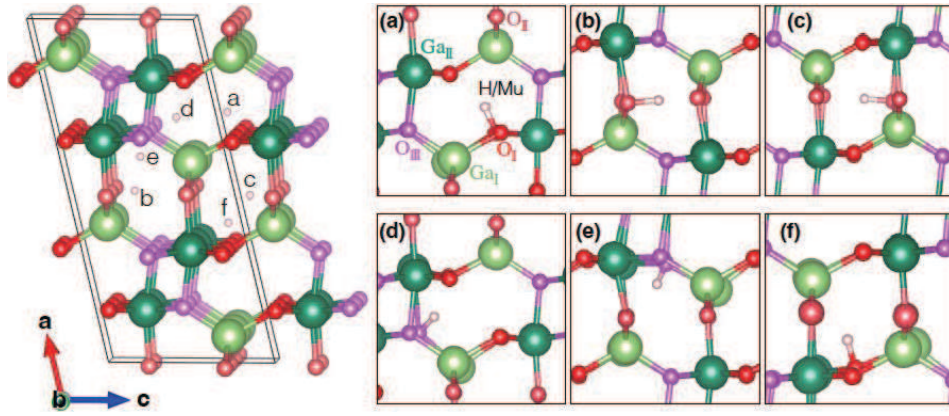


FIG. S3. Left: Crystal structure of β -Ga₂O₃. Isolated pink balls indicate the initial positions of hydrogen in the structural relaxation calculations shown in (a)-(f), respectively corresponding to H_I, H_{II}, H_{III}, H_{IV}, H_V, and H_{VI} in the Table S1. The crystal structures were drawn using VESTA [22]. The nuclear dipolar linewidth Δ calculated for each structure is shown in Table S1.

2×1 superlattice. Figure S4 shows the variation of the total energy,

$$\Delta E_{\text{tot}} \equiv E_{\text{tot}}(\mathbf{r}) - E_{\text{min}},$$

where \mathbf{r} is the position vector of channel c_i ($i = 1, 2, 3$) and E_{min} is the global minimum of $E_{\text{tot}}(\mathbf{r})$. Here, \mathbf{r} for $c_1 = (0.25, y, 0)$, $c_2 = (0.5, y, 0.5)$ and $c_3 = (0.5, y, 0)$, respectively. The ΔE_{tot} of c_2 and c_3 show large changes of more than 0.5 eV, whereas the ΔE_{tot} of c_1 is almost independent of y and the difference is only 0.04 eV, suggesting that c_1 is a the possible diffusion path for Mu₂.

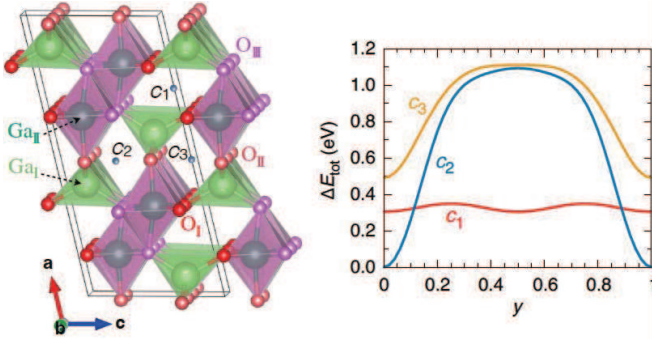


FIG. S4. Hydrogen position on the $\langle 010 \rangle$ axis dependence of the total energy calculated at the center c_i ($i = 1, 2, 3$) of each channel, shown in left panel, using the $1 \times 2 \times 1$ structure.

IV. SUPPLEMENTAL μ SR RESULTS

A. μ SR results on powder Sample

μ SR measurements and data analysis for the powder sample were performed as for the single crystal. The temperature dependence of each parameter obtained by curve fitting of the μ SR time spectra is shown in Fig. S5. For comparison, the results for the single-crystal sample presented in the

main text are also shown. As can be seen in Fig. S5(a), the

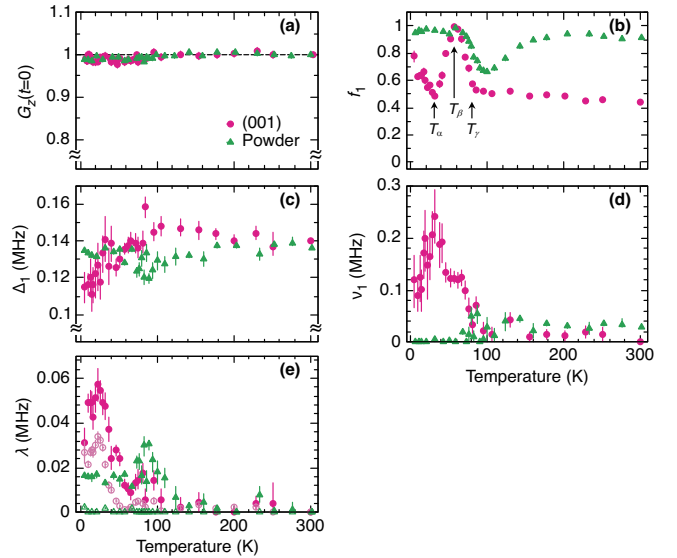


FIG. S5. Temperature dependence of (a) $G_z(0)$ determined by TF- μ SR, (b) the fractional yield f_1 , (c) the Kubo-Toyabe linewidth Δ_1 , (d) the fluctuation rate ν_1 , and (e) the exponential relaxation rate λ for the Mu₁ component. The result for the single crystalline sample is quoted from the main text for comparison.

most significant difference is that the yield f_1 of the Mu₁ component in the powder sample is greatly increased in place of the Mu₂ component. In addition, it is observed for the powder sample that ν_1 (the fluctuation rate of Δ_1) is almost zero (static) for $T \lesssim T_\gamma \simeq 80$ K, whereas it takes on finite values for $T \gtrsim T_\gamma$, suggesting slow diffusive motion of the Mu₁ component. These behaviors are in remarkable contrast to the single-crystal sample. On the other hand, the increase in f_1 (decrease in f_2) from T_β ($\simeq 55$ K) to T_γ is common. From these observations, it may be interpreted that for $T < T_\beta$, the component corresponding to Mu₂ in the powder sample is bounded by some defects, etc., and that a part of it is detrapped and begins

to exhibit fast diffusion for $T_\beta < T < T_\gamma$, which is gradually suppressed above T_γ .

B. Comparison of curve fits for the data around T_β

To test the possibility that quasi-static Mu_1 and Mu_2 co-exist in the μSR spectrum near the temperature at which f_2 decreases significantly, we performed global curve fits for the ZF and LF- μSR spectra with the linewidth Δ_1 and Δ_2 as free parameters in each state, as well as for those fixed to the values expected for the corresponding sites ($\Delta_1 = 0.136$ MHz and $\Delta_2 = 0.345$ MHz). The results of the respective analyses for the spectra at 57 K are shown below in Fig. S6(a) and (b). The fits with Δ fixed to the expected values at the two sites show large residual chi-squares, clearly indicating that the data are

not well reproduced.

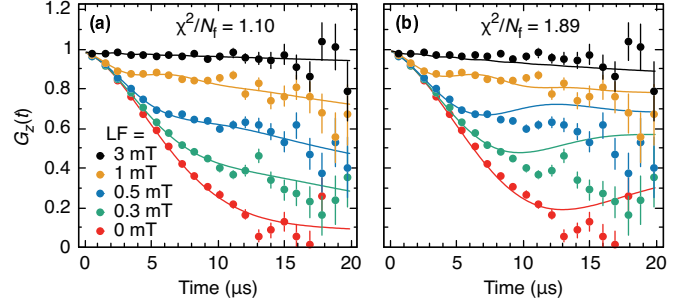


FIG. S6. Analyzed μSR spectra at 57 K (global fit of the entire ZF/LF data). (a) with Δ_1 and Δ_2 as free parameters, (b) fixed to $\Delta_1 = 0.136$ MHz and $\Delta_2 = 0.345$ MHz.